Topochemistry

DOI: 10.1002/anie.201309460

The Topochemical Pseudomorphosis of a Chloride into a Bismuthide**

*Martin Kaiser, Bertold Rasche, and Michael Ruck**

Abstract: *The heterogeneous reaction of crystals of the novel intermetallic subhalide $Bi_{12}Rh_3Cl_2$ with a solution of n-butyllithium at 70°C led to the complete topochemical exchange of chloride ions for bismuth atoms, that is, the transformation into the isostructural metastable intermetallic superconductor $Bi_{14}Rh_3$. The crystals underwent the reductive pseudomorphosis almost unchanged except some fissures perpendicular to the a-axis. Detailed inspections of the transformed crystals by electron microscopy indicated no volume defects that would indicate internal chemical reactions. Thus, extensive mass transport must have occurred through the seemingly dense crystal structure. An efficient transport mechanism, based on an unusual breathing mode of the three-dimensional network formed by edge-sharing [RhBi$_8$] cubes and antiprisms, is proposed. The replacement of ionic interaction in the chloride by metallic bonding in the binary intermetallic compound closes the pseudo gap in the density of states at the Fermi level. As a result, the rod-packing of conducting, yet electrically isolated strands of [RhBi$_8$] cubes in $Bi_{12}Rh_3Cl_2$ turns into the three-dimensional metal $Bi_{14}Rh_3$.*

Ion exchange is a familiar and widely exploited phenomenon that requires materials with high surface area, such as resins, zeolites, or clays. Compact crystalline structures of intermetallic compounds seem to be unsuitable for such reactions since they contain no paths for efficient mass transport. Thus all the more surprising is the observation of a complete topochemical ion exchange that transforms a $Bi_{12}Rh_3Cl_2$ crystal into a $Bi_{12}Rh_3Bi_2$ ($=Bi_{14}Rh_3$)[1] crystal in a solution of *n*-butyllithium (*n*BuLi) at only 70°C. To understand how this intriguing exchange became possible, an extensive analysis of the crystal chemistry is necessary.

The starting material, $Bi_{12}Rh_3Cl_2$ (Figure 1), is a new member of the compound class of bismuth-rich subhalides that include elements of Groups 8 to 10.[2] A common characteristic of these compounds are strong metal–metal bonds, especially between bismuth and the transition metal. The thereby formed intermetallic substructures range from clusters to three-dimensional networks, depending on the halogen content, that is, the degree of oxidation of the intermetallic part. Examples relevant for the following are the layered compounds $Bi_{13}Pt_3I_7$[3] and $Bi_{14}Rh_3I_9$.[4] They feature kagomé nets of edge-sharing [MBi$_8$] cubes (M = Rh, Pt) and are regarded as pseudo two-dimensional metals. Besides, $Bi_{14}Rh_3I_9$ is the first example of a weak topological insulator.[5] The lowest halogen content to date was found in $Bi_{12}Rh_3Br_2$ and the isostructural chloride presented herein,[6] whose three-dimensional metallic networks are formed by edge-sharing [RhBi$_8$] cubes and antiprisms (Figure 1).

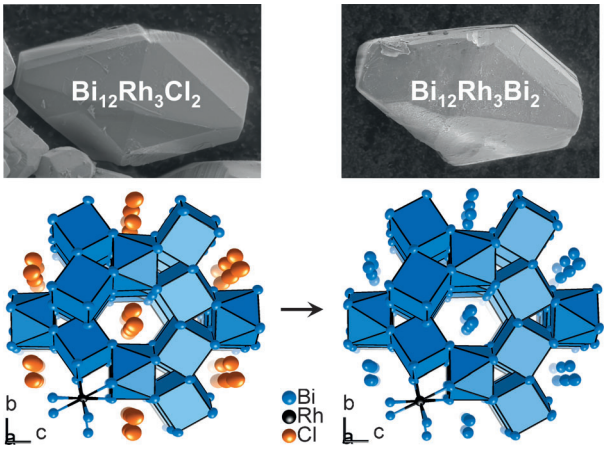

Figure 1. SEM micrographs and sections of the crystal structures of the starting material $Bi_{12}Rh_3Cl_2$ (left) and of the product of the transformation $Bi_{12}Rh_3Bi_2$ ($=Bi_{14}Rh_3$,[1] right). The intermetallic frameworks are formed by strands of edge-sharing [RhBi$_8$] cubes that are linked by rhodium atoms in square-antiprismatic coordination. Additional atoms X = Cl or Bi fill the channels along the *a*-axis. Ellipsoids represent 99% probability.

Some of the intermetallic motifs of the subhalides are also stable in their non-oxidized states. For example $^1_\infty$[Bi_3Ni] strands, present in $Bi_{12}Ni_4I_3$, also constitute the binary intermetallic Bi_3Ni.[7] The structural analogy demonstrates tolerance for changes in the electron count of the intermetallic part and provides options for redox chemistry. Hence, we developed a new method[8] that uses *n*-butyllithium (*n*BuLi) to remove the halide ions from the subhalides under mild conditions (boiling hexane, 70°C) while the intermetallic parts are preserved. The resulting non-crystalline assemblies of parallel $^1_\infty$[Bi_3Ni] nanofibers have physical properties distinct from bulk Bi_3Ni, showing a rare case of the coexistence of superconductivity and ferromagnetism.[9,10] We further applied this mild reductive process to subiodides that contain intermetallic substructures unknown from intermetallic phases: $Bi_{28}Ni_{25}I_5$ and $Bi_8Ni_8SI_2$ were dehalogenated in topochemical reactions to crystalline but metastable $Bi_{28}Ni_{25}$[11] and Bi_8Ni_8S.[12]

[*] M. Kaiser, B. Rasche, Prof. Dr. M. Ruck
Fachrichtung Chemie und Lebensmittelchemie
Technische Universität Dresden
01062 Dresden (Germany)
E-mail: michael.ruck@tu-dresden.de
Prof. Dr. M. Ruck
Max-Planck-Institut für Chemische Physik fester Stoffe
Nöthnitzer Strasse 40, 01187 Dresden (Germany)

[**] We gratefully acknowledge Dr. I. Kunert (TU Dresden) for DSC measurements, Dr. G. Auffermann (MPI CPfS) for chemical analyses. We are indebted to ZIH TU Dresden for the provided computational facilities.

Supporting information for this article is available on the WWW under http://dx.doi.org/10.1002/anie.201309460.

Attempts to de-intercalate the bromide ions out of the three-dimensional intermetallic network of $Bi_{12}Rh_3Br_2$ yielded powders of a compound, which could not be characterized by X-ray diffraction owing to its poor crystallinity (Figure S1 in the Supporting Information). We assumed that a topochemical de-intercalation reaction might have occurred, but was in part destructive or remained incomplete because the channels along the *a*-axis, in which the bromide ions reside (Figure 1), are not wide enough for diffusion. The to date unknown subchloride $Bi_{12}Rh_3Cl_2$ was presumed to have virtually the same channel diameter but smaller and thus more mobile anions.

The direct transfer of the synthetic method for $Bi_{12}Rh_3Br_2$ to the chloride proved unsuccessful. A new route was developed that uses Bi_4Rh (decomposition temperature: 466 °C)[13] instead of elemental rhodium (melting point: 1964 °C). For optimization, the reaction was monitored by differential scanning calorimetry (DSC). Upon heating, a mixture of Bi_4Rh and $BiCl_3$ shows overlapping endo- and exothermic signals in a wide temperature range from 200 °C to 350 °C (Figure 2). Through thermal activation and melting

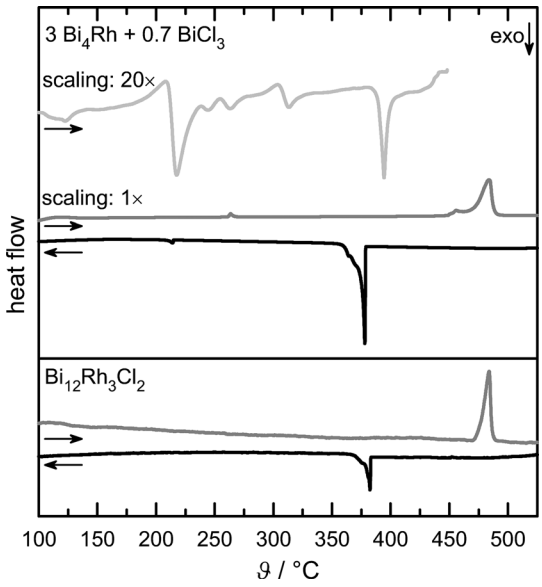

Figure 2. Thermal analysis (DSC) of a powdered mixture of Bi_4Rh and $BiCl_3$ (top; molar ratio 3:0.7, small excess of bismuth) and a phase pure sample of $Bi_{12}Rh_3Cl_2$ (bottom). The first heating of the mixture (light gray line) was aborted at 450 °C and a second DSC scan up to 550 °C was performed on the same sample after cooling to room temperature (heating: dark gray line; cooling: black line).

of $BiCl_3$ a small amount of Bi_4Rh is oxidized and some α-Bi_2Rh[14] is formed as a side product (Figure S2a). At 390(5) °C solid Bi_4Rh reacts with the chloride melt and forms solid $Bi_{12}Rh_3Cl_2$ (**1**) [Eq. (1); Figure S2b].

$$3\,Bi_4Rh + 0.7\,BiCl_3 \rightarrow Bi_{12}Rh_3Cl_2 + 0.7\,\text{“Bi”} \quad (1)$$

The formally remaining “bismuth” is in fact found in the bismuth-rich phase $Bi_{35}Rh_3Cl_{38}$.[2f] Compound **1** decomposes incongruently at 475(5) °C into bismuth, β-Bi_2Rh,[15] and $BiCl_3$ (Figure S2c), and crystallizes at 383(10) °C from this mixture. Compound **1** does not show any thermal effects below the decomposition temperature (Figure 2). Based on the results of thermal analysis, single-crystals for structure determination have been grown.

Compound **1** forms diamond shaped crystals with a metallic luster and is isostructural to $Bi_{12}Rh_3Br_2$. All lattice parameters of **1** are approximately 1 % smaller than for the bromide, whereas the average Bi–Rh distance is only 0.4 % shorter (Table S1, S2). Although the anion-containing channels along the *a*-axis are contracted compared to the bromide, large displacement parameters of the chloride ion ($U_{eq}(Cl) = 411(5)$ pm^2; $U_{eq}(Br) = 273(3)$ pm^2; Table S2) indicate mobility about its center of gravity (Figure 1).

As had been expected, the chloride ions can be extracted by treating crystals of **1** with an excess of *n*BuLi at 70 °C. But surprisingly, the reductive topochemical de-intercalation of chloride ions is accompanied by the topochemical intercalation of bismuth atoms into the crystal structure to fill the voided positions. The isostructural metastable superconductor[13] $Bi_{12}Rh_3Bi_2$ ($= Bi_{14}Rh_3$;[1] (**2**)) is obtained (Figure S2d). The crystals of **1** are not dissolved in the course of the reaction. While the crystals' shapes remain nearly unchanged after reductive pseudomorphosis, some cracks and fissures appear perpendicular to the *a*-axis (Figure 3 and Figure S3). Correspondingly, X-ray diffractograms (XRD) of **2** show broadening of reflections with high *h* indices (Figure S2d).

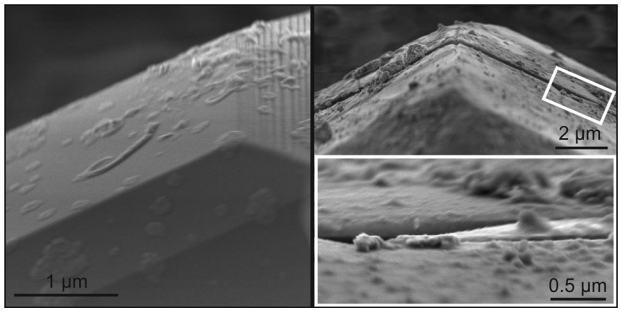

Figure 3. SEM micrographs of the edges of single crystals of the starting material $Bi_{12}Rh_3Cl_2$ (left) and the product of the topochemical redox reaction $Bi_{14}Rh_3$ (right).

Detailed inspection of the product crystals by scanning and transmission electron microscopy (SEM, TEM) indicate no volume defects that would indicate internal chemical reactions. Thus, the entire transformation must be based on efficient transport of chloride ions out and bismuth atoms into the framework. According to XRD and TEM investigations the topochemical exchange is complete. Energy-dispersive X-ray spectroscopy (EDX) on small crystals confirmed the composition (Bi: 83 at.%; Rh: 17 at.%; no chlorine; Figure S4), and chemical analyses verified the absence of lithium in **2**. The onset temperature of the kinetically controlled exothermic decomposition of **2** (150(5) °C; Figure S5) is lower than for conventionally synthesized samples (173 °C),[13] and in addition to Bi_4Rh some α-Bi_2Rh is formed instead of the expected bismuth.[13]

As the transformed crystals were essentially undamaged, we were able to determine the crystal structure of **2** by X-ray diffraction on a single-crystal. The interatomic distances do not differ by more than 1.1 pm from the reported values.[1] One of the most prominent differences between the structures of **1** and **2** concerns the torsion angle of the [$RhBi_8$] square antiprisms (Figure 4 and Table 1). Correlated to it, the inclination (ω) and the distance (d) between the strands of edge sharing [$RhBi_8$] cubes that run along [110] and [−110] are changed. Hence, the [$RhBi_8$] antiprisms act as hinges in the framework.

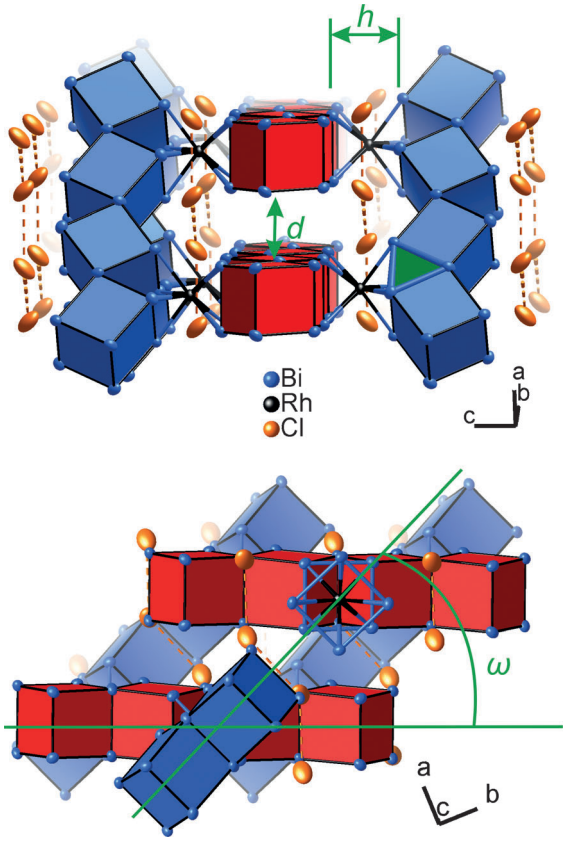

Figure 4. Intermetallic framework of $Bi_{12}Rh_3X_2$ (X = Cl, Br, Bi).The parallel oriented strands of [$RhBi_8$] cubes (blue along [110], red along [−110]) are cross-linked by [$RhBi_8$] square antiprisms. One of the triangles between edge-sharing [$RhBi_8$] polyhedra is marked in green.

From these considerations a reasonable mechanism for the enormous mass transport during the transformation process can be deduced. If the inclination is raised towards $\omega_{max} = 90°$ (i.e. the antiprism becomes a cube), wide diffusion paths up to $d_{max} = 583$ pm ($\Delta d_{max} = +252$ pm) will open up parallel to all the intermetallic strands. Additional deformation of the cubes in the strands may reduce the necessary increase of the torsion angle of the antiprisms. Since the diffusion paths intersect, the transport system is in fact three-dimensional. Cooperative extension and subsequent contraction of the crystal will predominantly affect the a-axis. This is in accordance with the above described crack formation perpendicular to the a-axis and the broadening of reflections

Table 1: Synopsis of structural data for $Bi_{12}Rh_3Cl_2$ (**1**) and $Bi_{14}Rh_3$ (**2**).

Parameter	$Bi_{12}Rh_3Cl_2$ (X=Cl)	$Bi_{12}Rh_3Bi_2$ (X=Bi)	change Δ
space group	*Fddd*	*Fddd*	
a [pm]	710.93(3)	690.02(3)	−2.9%
b [pm]	1665.74(7)	1736.16(7)	+4.2%
c [pm]	3161.3(1)	3169.4(1)	+0.3%
ρ_{calcd} [g cm^{-3}]	10.246	11.316	+10.4%
average Bi–Rh distance [pm]	283.8	285.8	+0.7%
average Bi–Bi distance [pm]	329.3	333.2	+1.2%
average Bi···X distance [pm]	341.4	345.9	+1.3%
X···X distance [pm]	378.7(1)	361.89(5)	−4.4%
$\omega = arctan(a/b) \times 2$	46.1°	43.3°	−6.2%
torsion angle of [$RhBi_8$] antiprisms	43.6°	40.5°	−7%
distance d between adjacent strands of [$RhBi_8$] cubes [pm]	331	323	−2.4%
height h of [$RhBi_8$] antiprisms [pm]	331.2	332.8	+0.5%

with high h component. Furthermore, it was verified on a self-made 3D-model of the polyhedra framework.

Although, the intermetallic network is only slightly changed, the electronic situations, as calculated based on full-relativistic density functional theory (DFT), in **1** and **2** are quite different. For the halides $Bi_{12}Rh_3X_2$ (X = Cl, Br), the density of states (DOS) reveals a pseudo gap at the Fermi level (Figure 5, left; for X = Br see Figure S6b). Its origin can be found by analyzing two special directions in the real structure (Figure 5, left; X = Br and other directions in

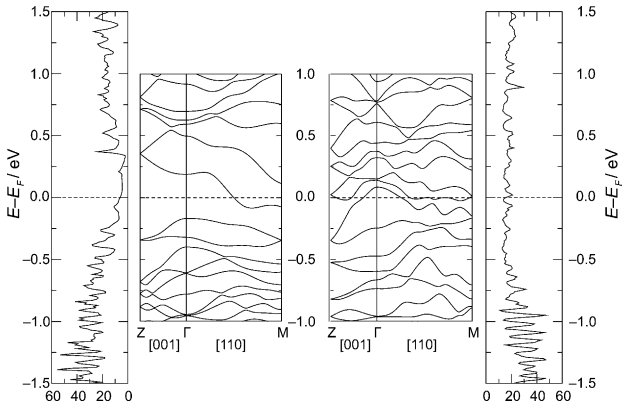

Figure 5. Density of states (DOS) and electronic band structure along selected directions for $Bi_{12}Rh_3Cl_2$ (left) and $Bi_{14}Rh_3$ (right).

Figure S7). Along the Γ–M direction, which can be associated with the direction of the strands of [$RhBi_8$] cubes parallel to [110], a band with strong dispersion crosses the Fermi level. In contrast, perpendicular to all the strands (i.e. [001]), along the Γ–Z direction, insulating behavior is observed. To understand this electronic signature, a comparison to the electronic situation of the structurally related compound $Bi_{14}Rh_3I_9$ helps. In $Bi_{14}Rh_3I_9$, the states close to the Fermi level are attributed to delocalized electrons in triangles between the edge-sharing [$RhBi_8$] cubes.[5] The same triangles exist within the strands of

[$RhBi_8$] cubes in $Bi_{12}Rh_3X_2$ (Figure 4, marked in green). These co-planar "triangle-states" couple and hence the strands become metallic along the Γ–M direction. Along the *c*-axis, the triangles are not in the same plane and coupling is impossible. The gap along the Γ–Z direction shows that no alternative pathway for electrons exists. In other words, the [$RhBi_8$] antiprisms are centers of electronic localization and isolate the conducting strands of [$RhBi_8$] cubes from each other.

For the transformed structure **2** with bismuth atoms replacing halide ions, the situation in the metallic Γ–M direction is qualitatively unchanged. The previously insulating Γ–Z direction, however, changes drastically, as numerous bands now cross the Fermi level (Figure 5, right). The additional bismuth atoms in the channels efficiently connect adjacent strands (distance $Bi_{framework}$–$Bi_{channel} \geq 338.5$ pm; 345.9 pm in average) and a new pathway for conductivity arises along the *c*-axis. Consequently, the DOS for $Bi_{14}Rh_3$ no longer shows a pseudo gap at the Fermi level but is almost constant above −0.5 eV (Figure 5, right). In other words, the ionic interaction in the halides is replaced by mainly metallic bonding in the binary intermetallic compound. Thereby the strands of [$RhBi_8$] cubes become interconnected electronically and a three-dimensional metal results.

A comparison of Mulliken charges supports this conclusion. Whereas the rhodium atoms have charges of about −0.3 in all three structures (X = Cl, Br, Bi), for the bismuth atoms of the framework and the atoms in the channels the charges differ. The halide ions (Cl: −0.6; Br: −0.5) induce a positive charge of about +0.2 on the bismuth atoms in the framework. In $Bi_{14}Rh_3$, the charges for all the bismuth atoms are almost zero. The bismuth atoms in the framework experience only a weak positive polarization (about +0.08) because of the electrophilic rhodium atoms. The bismuth atoms in the channels bear a small negative charge (−0.04). A similar finding based on previous scalar-relativistic calculations has led to the interpretation as a bismuthide.[1]

Experimental Section

Synthesis: All starting materials and products were handled in an argon-filled glove box (M. Braun; $p(O_2)/p^0 < 1$ ppm, $p(H_2O)/p^0 <$ 1 ppm). Bi_4Rh was synthesized by annealing a stoichiometric mixture of rhodium (99.95%, ChemPur, particle size ≤20 μm) and bismuth (99.9999%, ChemPur, treated with H_2 at 220 °C). Temperature program: +130 K h^{-1} from room temperature to 280 °C; +0.83 K h^{-1} to 300 °C; +65 K h^{-1} to 430 °C; annealing for 12 days; −17 K min^{-1} to room temperature. $BiCl_3$ (98%, Alfa Aeser) was purified by sublimation (two times). Hexane was pre-dried over calcium chloride, then distilled from sodium hydride dispersion and stored over activated 4 Å molecular sieves. Ethanol was distilled after reaction with sodium and diethyl phthalate and stored over activated 3 Å molecular sieves. The concentration of *n*-butyllithium in hexane was determined employing 4-(hydroxymethyl)biphenyl as an indicator.

1 ($Bi_{12}Rh_3Cl_2$): The synthesis conditions were derived from preceding thermal analysis experiments. Bi_4Rh and $BiCl_3$ (molar ratio 3:0.7; 100 mg starting materials per mL volume of the ampoule) were mixed and sealed in an evacuated ($p \leq 0.1$ Pa) silica ampoule. Temperature program: +5 K min^{-1} from room temperature to 450 °C; annealing for 14 d; −1 K min^{-1} to 300 °C and −10 K min^{-1} to room temperature.

2 ($Bi_{14}Rh_3$): The reaction was performed in flame-dried glassware under an atmosphere of argon. Liquid reagents were transferred by means of syringe. Crystals of **1** (0.01 mmol) were covered with dry hexane (10 mL). A hexane-based solution of *n*BuLi (0.1 mL; Sigma Aldrich; 1.6 mol L^{-1}; 15 equivalents with respect to **1**) were injected. After two days at 70 °C, the liquid phase of the heterogeneous mixture was removed with a syringe and the remaining solid was washed several times with absolute ethanol. Drying was performed in dynamic vacuum ($p \leq 0.1$ Pa). Compounds **1** and **2** are inert to air, water, and alcohols.

Thermal and chemical analyses: Thermal analyses were performed under equilibrium pressure (sealed silica ampoule) using a DTA-DSC Labsys TMA System (Setaram) at 10 K min^{-1} heating and cooling rates. Chemical analysis of a powdered sample by ICP-OES, ICP-MS, and ion chromatography:

1: $Bi_{12}Rh_3Cl_2$ (atom %): calcd: Bi 70.6, Rh 17.6, Cl 11.8; found: Bi 69.5(5), Rh 17.3(3), Cl 13.3(3).

2: $Bi_{14}Rh_3$ (atom %): calcd: Bi 82.4, Rh 17.6; found: Bi 76.6(3), Rh 19.8(3), Cl 3.7(1). No lithium was detected.

Scanning electron microscopy and energy-dispersive X-ray spectroscopy: SEM micrographs have been collected on a Hitachi SU8020 with a triple detector system for secondary and low-energy backscattered electrons ($U_a = 2$ kV). EDX spectra were collected using an Oxford Silicon Drift Detector (SDD) X-Max^N.

X-ray crystallography: Apex-II kappa CCD diffractometer (Bruker); $Mo_{K\alpha}$ radiation, $\lambda = 71.073$ pm, $T = 296(1)$ K; numerical absorption corrections[16] based on optimized crystal descriptions;[17] structure solutions with direct methods and refinements against F_o^2.[18] The refined structure models (Table S1, S2) match the measured powder diffraction patterns ($Bi_{12}Rh_3Cl_2$: Figure S2 b; $Bi_{14}Rh_3$, Figure S2 d). Graphics of the structures were developed with Diamond.[19]

1: $Bi_{12}Rh_3Cl_2$: *Fddd* (no. 70), $a = 710.93(3)$, $b = 1665.74(7)$, $c =$ 3161.3(1) pm, $V = 3743.7(3) \times 10^6$ pm^3; $Z = 8$; $\rho_{calcd} = 10.25$ g cm^{-3}; $\mu(Mo_{K\alpha}) = 115.2$ mm^{-1}; $2\theta_{max} = 77.90°$; 23 635 measured, 2597 unique reflections, $R_{int} = 0.056$, $R_\sigma = 0.033$; 43 parameters; extinction coefficient $1.11(2) \times 10^{-4}$; $R_1[2118\ F_o > 4\sigma(F_o)] = 0.019$, wR_2(all F_o^2) = 0.026, $GooF = 0.97$; min./max. residual electron density: −1.62/ 1.92 e × 10^{-6} pm^{-3}.

2: $Bi_{14}Rh_3$: *Fddd* (no. 70), $a = 690.02(3)$, $b = 1736.16(7)$, $c =$ 3169.4(1) pm, $V = 3796.9(3) \times 10^6$ pm^3; $Z = 8$; $\rho_{calcd} = 11.32$ g cm^{-3}; $\mu(Mo_{K\alpha}) = 131.7$ mm^{-1}; $2\theta_{max} = 54.98°$; 8094 measured, 1075 unique reflections, $R_{int} = 0.055$, $R_\sigma = 0.029$; 42 parameters; $R_1[855\ F_o > 4\sigma(F_o)] = 0.027$, wR_2(all F_o^2) = 0.059, $GooF = 1.08$; min./max. residual electron density: −2.10/2.60 e × 10^{-6} pm^{-3}.

Further details on the crystal structure investigations may be obtained from the Fachinformationszentrum Karlsruhe, 76344 Eggenstein-Leopoldshafen, Germany (fax: (+49) 7247-808-666; e-mail: crysdata@fiz-karlsruhe.de), on quoting the depository numbers CSD-426891 (**1**) and -426890 (**2**).

Quantum chemical calculations: DFT based calculations were performed with the Full-Potential-Local-Orbital (FPLO) code[20] version 9.01, within the local density approximation (LDA).[21] For full-relativistic calculations the four-component Dirac equation was solved. The Blöchl corrected linear tetrahedron method with a 12 × 12 × 12 *k*-mesh was employed for integration. The following basis states were treated as valence states: **Bi**: 5s, 5p, 5d, 6s, 6p, 6d, 7s, 7p; **Rh**: 4s, 4p, 4d, 5s, 5p, 5d, 6s; **Cl**: 2s, 2p, 3s, 3p, 3d, 4s, 4p; **Br**: 3s, 3p, 3d, 4s, 4p, 4d, 5s, 5d. M is the point on the boarder of the first Brillouin

zone in the real space direction [110]. The coordinates of M with respect to the primitive reciprocal cell are (0.5; 0.079; 0.579)/2π.

Received: October 30, 2013
Revised: December 20, 2013
Published online: February 12, 2014

Keywords: intermetallic phases · metastable compounds · subvalent compounds · synthetic methods · topochemistry

[1] Q. F. Gu, G. Krauss, Yu. Grin, W. Steurer, *J. Solid State Chem.* **2007**, *180*, 940 – 948.
[2] a) M. Ruck, *Angew. Chem.* **2001**, *113*, 1222 – 1234; *Angew. Chem. Int. Ed.* **2001**, *40*, 1182 – 1193; b) M. Ruck, *Z. Kristallogr.* **2010**, *225*, 167 – 172; c) M. Ruck, *Z. Anorg. Allg. Chem.* **1997**, *623*, 1591 – 1598; d) M. Ruck, *Z. Anorg. Allg. Chem.* **1998**, *624*, 521 – 528; e) M. Ruck, *Z. Anorg. Allg. Chem.* **2000**, *626*, 14 – 22; f) M. Ruck, S. Hampel, *Polyhedron* **2002**, *21*, 651 – 656; g) S. Hampel, M. Ruck, *Z. Anorg. Allg. Chem.* **2006**, *632*, 1150 – 1156; h) F. Steden, P. Schmidt, B. Wahl, A. Isaeva, M. Ruck, *Z. Anorg. Allg. Chem.* **2008**, *634*, 69 – 76; i) A. Günther, F. Steden, M. Ruck, *Z. Anorg. Allg. Chem.* **2008**, *634*, 423 – 430; j) M. Ruck, *Angew. Chem.* **1997**, *109*, 2059 – 2062; *Angew. Chem. Int. Ed. Engl.* **1997**, *36*, 1971 – 1973; k) M. Ruck, *Z. Anorg. Allg. Chem.* **1997**, *623*, 1583 – 1590; l) M. Ruck, R. M. Heich, *Z. Anorg. Allg. Chem.* **2000**, *626*, 2449 – 2456; m) M. Ruck, *Z. Anorg. Allg. Chem.* **1997**, *623*, 243 – 249; n) M. Ruck, *Z. Anorg. Allg. Chem.* **1999**, *625*, 453 – 462; o) B. U. Wahl, Th. Doert, T. Söhnel, M. Ruck, *Z. Anorg. Allg. Chem.* **2005**, *631*, 457 – 467; p) B. Wahl, M. Ruck, *Acta Crystallogr. Sect. B* **2009**, *65*, 593 – 599; q) B. Wahl, L. Kloo, M. Ruck, *Z. Anorg. Allg. Chem.* **2009**, *635*, 1979 – 1985; r) A. I. Baranov, L. Kloo, A. V. Olenev, B. A. Popovkin, A. I. Romanenko, A. V. Shevelkov, *J. Am. Chem. Soc.* **2001**, *123*, 12375 – 12379; s) A. I. Baranov, L. Kloo, A. V. Olenev, B. A. Popovkin, A. I. Romanenko, *Inorg. Chem.* **2003**, *42*, 3988 – 3993; t) M. Ruck, *Z. Anorg. Allg. Chem.* **1995**, *621*, 2034 – 2042.
[3] M. Ruck, *Z. Anorg. Allg. Chem.* **1997**, *623*, 1535 – 1541.
[4] B. Rasche, A. Isaeva, A. Gerisch, M. Kaiser, W. V. d. Broek, C. T. Koch, U. Kaiser, M. Ruck, *Chem. Mater.* **2013**, *25*, 2359 – 2364.
[5] B. Rasche, A. Isaeva, M. Ruck, S. Borisenko, V. Zabolotnyy, B. Büchner, K. Koepernik, C. Ortix, M. Richter, J. van den Brink, *Nat. Mater.* **2013**, *12*, 422 – 425.
[6] M. Ruck, *Solid State Sci.* **2001**, *3*, 369 – 376.
[7] M. Ruck, T. Söhnel, *Z. Naturforsch. B* **2006**, *61*, 785 – 791.
[8] R. Boldt, M. Kaiser, D. Köhler, F. Krumeich, M. Ruck, *Nano Lett.* **2010**, *10*, 208 – 210.
[9] R. Boldt, A. Grigas, M. Heise, T. Herrmannsdörfer, A. Isaeva, S. Kaskel, D. Köhler, M. Ruck, R. Skrotzki, J. Wosnitza, *Z. Anorg. Allg. Chem.* **2012**, *638*, 2035 – 2043.
[10] T. Herrmannsdörfer, R. Skrotzki, J. Wosnitza, D. Köhler, R. Boldt, M. Ruck, *Phys. Rev. B* **2011**, *83*, 140501.
[11] M. Kaiser, A. Isaeva, M. Ruck, *Angew. Chem.* **2011**, *123*, 6302 – 6304; *Angew. Chem. Int. Ed.* **2011**, *50*, 6178 – 6180.
[12] M. Kaiser, A. Isaeva, R. Skrotzki, U. Schwarz, M. Ruck, *Z. Anorg. Allg. Chem.* **2011**, *637*, 2026 – 2032.
[13] F. Weitzer, W. Schnelle, R. C. Gil, S. Hoffmann, R. Giedigkeit, Y. Grin, *CALPHAD Comput. Coupling Phase Diagrams Thermochem.* **2009**, *33*, 27 – 30.
[14] a) R. N. Kuz'min, G. S. Zhdanov, *Sov. Phys. Crystallogr.* **1961**, *6*, 704 – 711; b) A. Kjekshus, *Acta Chem. Scand.* **1971**, *25*, 411 – 422.
[15] M. Ruck, *Acta Crystallogr. Sect. B* **1996**, *52*, 605 – 609.
[16] a) X-RED32, *Data Reduction Program*, *Version 1.01*, Stoe & Cie GmbH, Darmstadt **2001**; b) V. Petricek, M. Dusek, L. Palatinus, JANA2006, *The Crystallographic Computing System*; Institute of Physics, Praha, Czech Republic, **2011**.
[17] X-Shape, Crystal Optimization for Numerical Absorption Correction Program, Version 2.12.2, Stoe & Cie GmbH, Darmstadt **2009**.
[18] a) G. M. Sheldrick, SHELX97, *Programs for crystal structure determination*, Release 97 – 2 Univ. Göttingen, **1997**; b) G. M. Sheldrick, SHELXTL XLMP, *Program for Crystal Structure Refinement – Multi-CPU Version 2013/2*, Bruker AXS Inc., Madison, WI, USA, **2013**; c) G. M. Sheldrick, *Acta Crystallogr. Sect. A* **2008**, *64*, 112 – 122.
[19] K. Brandenburg, *Diamond 3.2i*, Crystal Impact GbR, Bonn, **2012**.
[20] K. Koepernik, H. Eschrig, *Phys. Rev. B* **1999**, *59*, 1743 – 1757.
[21] J. P. Perdew, Y. Wang, *Phys. Rev. B* **1992**, *45*, 13244 – 13249.

